New two in one magnetic fluorescent nanocomposites

Serena A. Corr, * [a] Yurii K. Gun'ko, [a] Stephen J. Byrne, [a] Alexios P. Douvalis [b], Munuswamy Venkatesan [b] and Robert D. Gunning [b]

[a] The Department of Chemistry, Trinity College, University of Dublin, Dublin 2, Ireland

[b] The Department of Physics, Trinity College, University of Dublin, Dublin 2, Ireland

1. INTRODUCTION

Magnetic and fluorescent nanomaterials are of immense importance in the field of biomedicine[1-3]. In particular, the use of magnetic fluids based on magnetite (Fe_3O_4) and maghemite (Fe_2O_3), as both diagnostic tools in the form of magnetic resonance imaging (MRI) contrast agents [4, 5] and as a method of hyperthermic cancer treatment, [6, 7] is one of the fastest growing areas of nanobiomedical research. Currently, fluorescent semiconducting nanoparticles (quantum dots) [8] have been show to be promising materials for bio-labelling, [9] noninvasive biological imaging,[10] and highly specific detectors in biological assays. [11] The combination of magnetic nanoparticles with the properties of fluorescent molecules is therefore an attractive prospect, enabling the engineering of a targeted-nanoscale device which can be manipulated within the body via an external magnetic field.

Porphyrins are well known to be very important biomedical materials with remarkable biocompatibility. In the past, they have been used as effective and efficient photosensitisers in photodynamic therapy, a technique whereby tumour tissue is destroyed by the uptake of dye and subsequent irradiation of visible light[12, 13]. While it has been recently reported that magnetite treated with copper phthalocyanine dyes may be employed in drug screening[14, 15], to the best of our knowledge, porphyrin-functionalised iron oxide nanocomposites are unexplored. In this work, we present new two in one fluorescent and magnetic nanoparticles prepared *via* the functionalisation of magnetite nanocrystals with porphyrin.

2. RESULTS AND DISCUSSION

There are many methods for the preparation of magnetic nanoparticles which have been previously reported, involving chemical coprecipitation, oxidation of amorphous iron powder, and sol-gel methods.[16-18] Recently we have developed a new, effective technique based on sol-gel and ultrasonic processing, for the preparation of superparamagnetic magnetite nanoparticles from novel metallorganic precursors. The main advantage of this method is that it is a very quick, one-step procedure for preparation of magnetic nanoparticles by hydrolysis and ultrasonic treatment of Fe(II) tert-butoxide precursor without any additional stabilising agent. By employing the Fe (II) heterometallic precursor[19] $[(THF)NaFe(OBu^t)_3]_2$ and sodium bromide, magnetic nanocrystals of magnetite were prepared via this sol-gel technique. During the hydrolysis of this precursor, sodium hydroxide is evolved, which results in a basic pH of 10. We reported that it is the presence of NaOH that results in the formation of nanocrystalline[20] magnetite (Fe_3O_4).

These nanocrystals were then treated with 4, 4', 4'', 4''',-(21H, 23H-Porphine-5, 10, 15, 20–tetrayl)tetrakis–(benzoic acid) (TCPP) (see Figure 2). The basis of these experiments is to react the peripheral –COOH groups of the porphyrin ligand with the Fe-OH groups present on the surface of the nanocrystals (See Scheme 1). We have also carried out several experiments between TCPP and amorphous magnetite nanoparticles prepared by previously reported methods[21] in order to display the stability of the crystalline derivatives. In this paper, we will outline the procedure for the successful preparation of new two-in-one TCPP-magnetite nanocrystalline composites and show that these new crystalline materials are preferable over their similarly prepared amorphous equivalents.

To confirm the presence of magnetite, Raman, IR and Mössbauer Spectroscopy were carried out on the magnetite nanocrystals prior to coating. For Raman, the characteristic peak at 667cm^{-1} was found for magnetite (see Figure 1). A FTIR spectrum of these nanocrystals carried out in CsI gives an OH stretch at 3430cm^{-1}, with a stretch for magnetite at ca. 570cm^{-1}.

Opto-Ireland 2005: Nanotechnology and Nanophotonics, edited by Werner J. Blau, David Kennedy, John Colreavy, Proc. of SPIE Vol. 5824 (SPIE, Bellingham, WA, 2005)
0277-786X/05/$15 · doi: 10.1117/12.604833

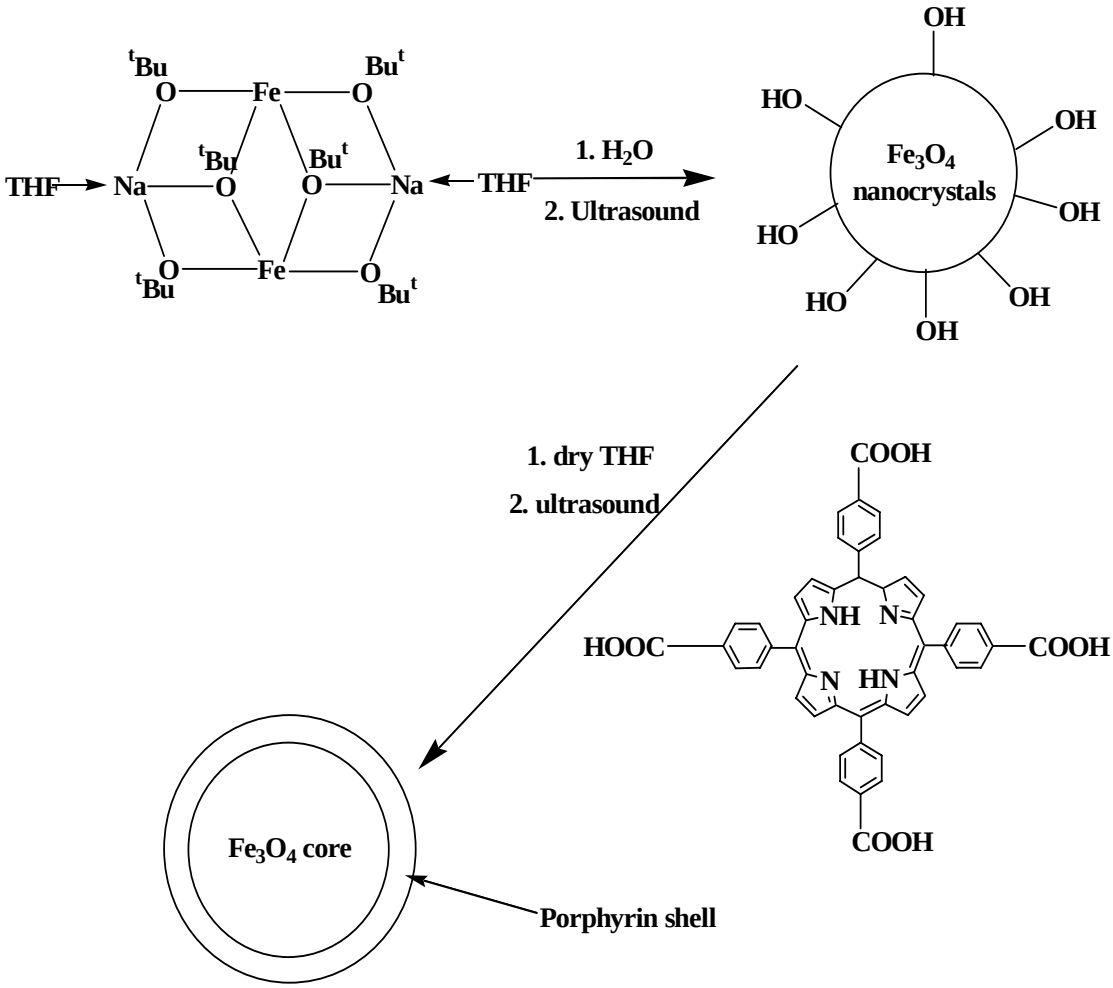

Scheme 1: Schematic representation for the formation of magnetite nanocrystals and subsequent porphyrin coating.

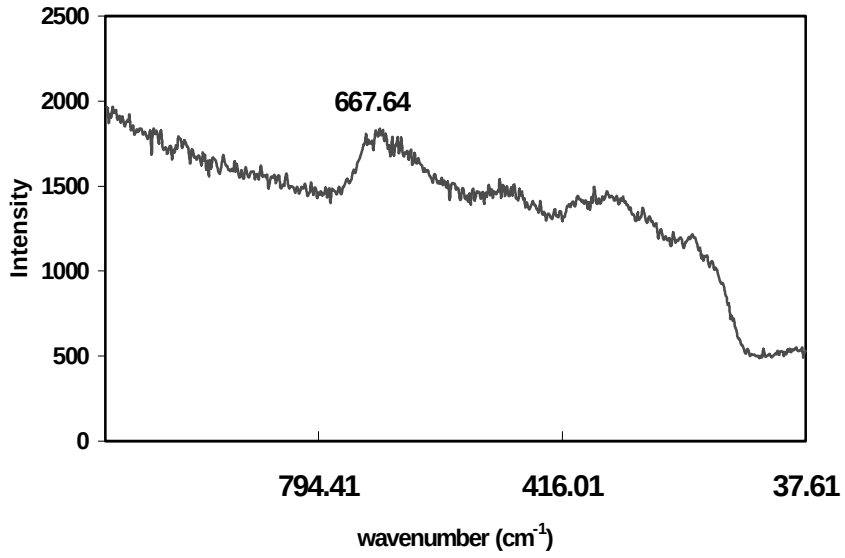

Figure 1: Raman spectrum of magnetite nanocrystals.

Because some techniques cannot be fully relied upon to distinguish between magnetite and maghemite, Mössbauer spectroscopy was employed (See Figure 2). Since Fe^{2+} only occurs in Fe_3O_4, the isomer shift in the spectrum is evidence of magnetite. Typical spectra obtained for the nanocrystalline samples are shown in figure 2. A set of five components was used to fit the room temperature spectrum. The resulting values of the Mössbauer parameters suggest the presence of magnetite nanocrystals with a distribution of different sizes. There are a pair of two well defined magnetically split sextets whose components correspond to the Fe^{3+} (A) and Fe^{2+}(B) sites of large, bulk like magnetite crystals (> 130 nm). This contribution is most likely from aggregates of the nanocrystals. There is a broad magnetically split sextet corresponding to small magnetite nanocrystals close to the superparamagnetic limit (6-10 nm). There is also a broad magnetically collapsing and one narrow superparamagnetic component with sizes of between 6 and 10 nm and below the superparamagnetic limit (< 6nm).

In order to assure that the spectrum is that of magnetite, a low temperature Mössbauer spectrum was obtained. At 150K, the spectrum was found to broaden and the central paramagnetic contribution is no longer present. This suggests a change in the superparamagnetic relaxation.

At 19K, the spectrum remains broad, with no indication of a superparamagnetic component. This spectrum is fit using one pair of components corresponding to the Fe^{3+} and Fe^{2+} ions.

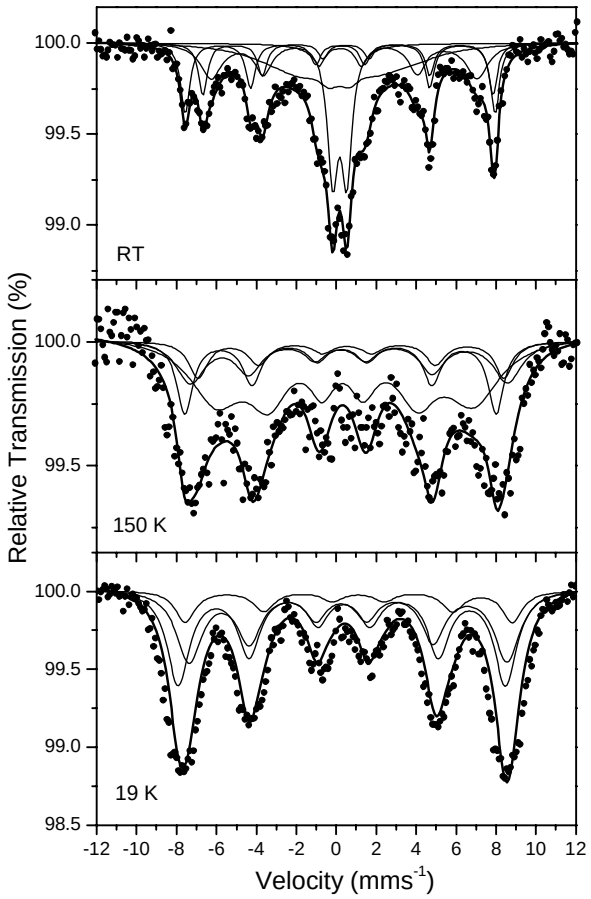

Fig. 2: Mössbauer spectra of magnetite nanocrystals collected at RT, 150 K, and 19 K.

Transmission Electron Microscopy (TEM) was employed to determine the average crystallite size, which was found to be 23 ± 5nm. The average sizes represented by a histogram reveal a narrow size distribution for these nanocrystals (see Figure 3).

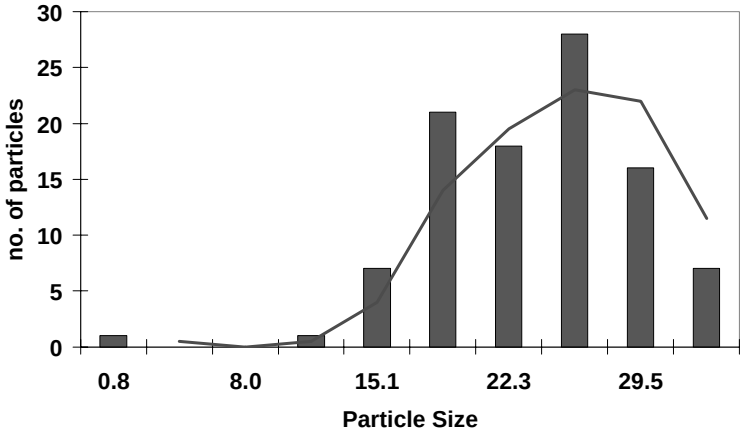

Figure 3: Average crystallite size calculated from TEM images

TEM images (see Figure 4) show the crystalline nature of these Fe_3O_4 magnetite nanoparticles. We have reported that this is the first room temperature synthesis of magnetite nanocrystals of this shape. SEM images also confirm the nano-crystalline morphology of this sample.

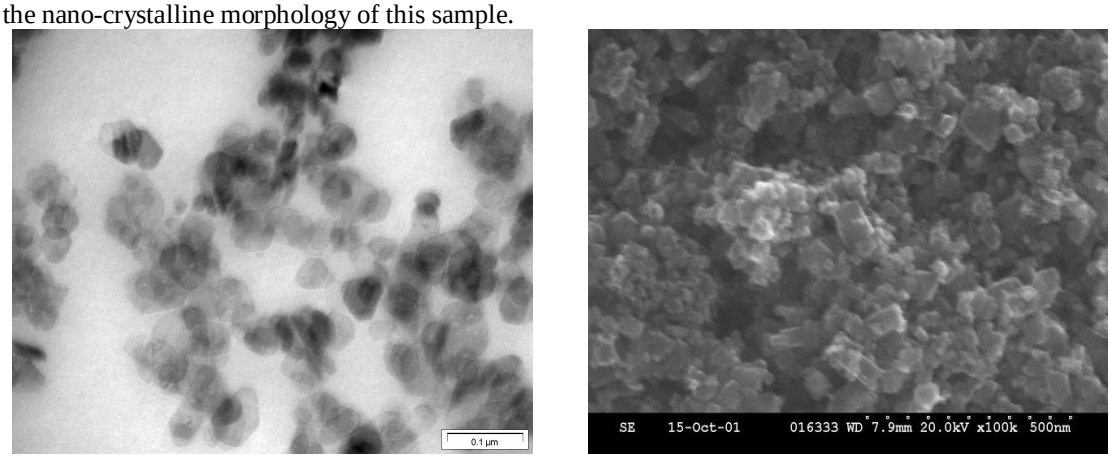

Figure 4: (a) TEM and (b) SEM images of magnetite nanocrystals.

The coating of these nanocrystals with TCPP was achieved via ultrasonic treatment of a suspension of the particles in dry THF with the porphyrin. The ultrasonic process involves the formation of cavitation bubbles, which may collapse or explode to produce localised areas of high temperature and pressure. We employ this technique to produce a reaction between our hydroxyl surface on the magnetite nanocrystals and the carboxylic acid groups of TCPP.

An IR spectrum for the magnetite nanocrystal-porphyrin composite does not show a stretch for the out of plane OC-OH group, which occurs at $964cm^{-1}$ in the porphyrin spectrum. This indicates the replacement of the porphyrin carboxylic acid group with an ester function between it and the OH groups of the magnetite.

TEM analysis (see Figure 5) reveals the formation of a core-shell nanocomposite, where the porphyrin coating is found to have an average thickness of 5nm. This gives evidence for the assembly of several molecular layers around the magnetite nanocrystals.

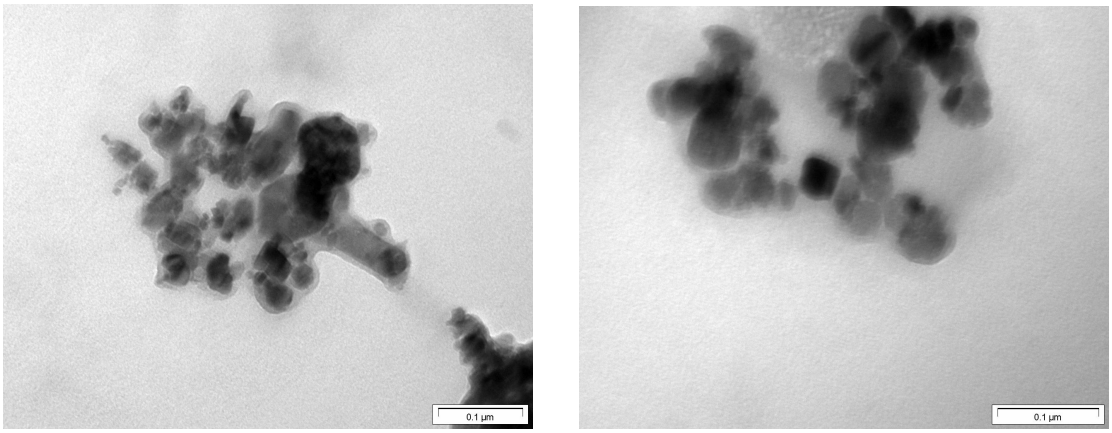

Figure 5: TEM images of the core-shell magnetite nanocrystal-TCPP composites.

In order to elucidate whether indeed we have porphyrin molecules bound to the particle surface, we carried out photochemical investigations. UV-vis spectrum in THF at pH 7 shows the characteristic Soret band maximum at 418nm. The Q-bands are more difficult to resolve as the spectrum is broadened by the presence of the nanocrystals, which act to scatter the light.

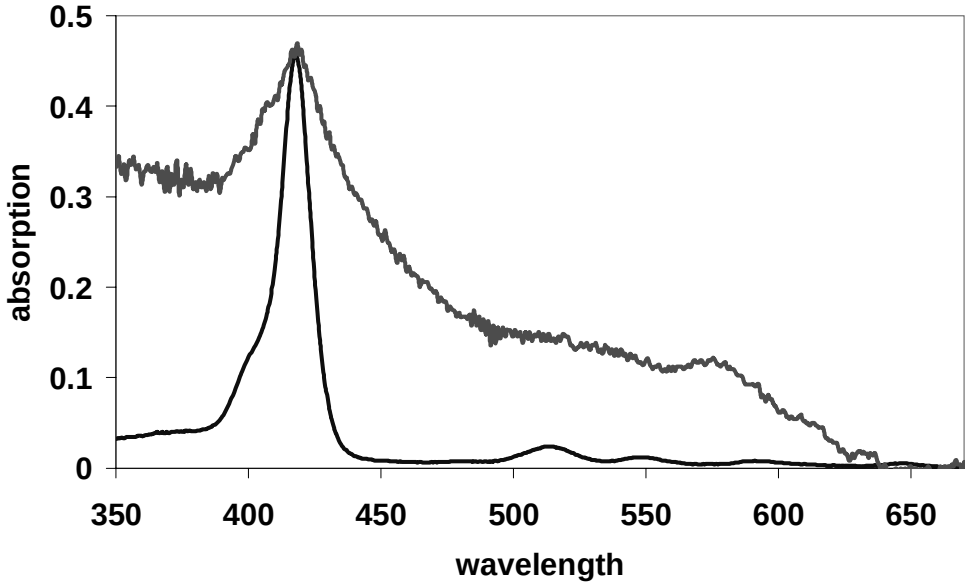

Figure 6: Absorption spectrum of TCPP in THF at pH 7 (bottom blue line) and magnetite nanocrystal-TCPP nanocomposite (top red line)

Fluorescence spectroscopy (see Figure 7) was carried out on the composite material to determine if the paramagnetic core quenched the luminescence. However, as TEM images revealed several layers of TCPP on the surface of the nanocrystals it was hoped that the emission of the TCPP would still be observed. Spectra carried out in THF revealed an emission band at 652 nm (compared with 654 nm for TCPP alone) and a corresponding excitation peak at 418 nm (compared with 422 for TCPP alone).

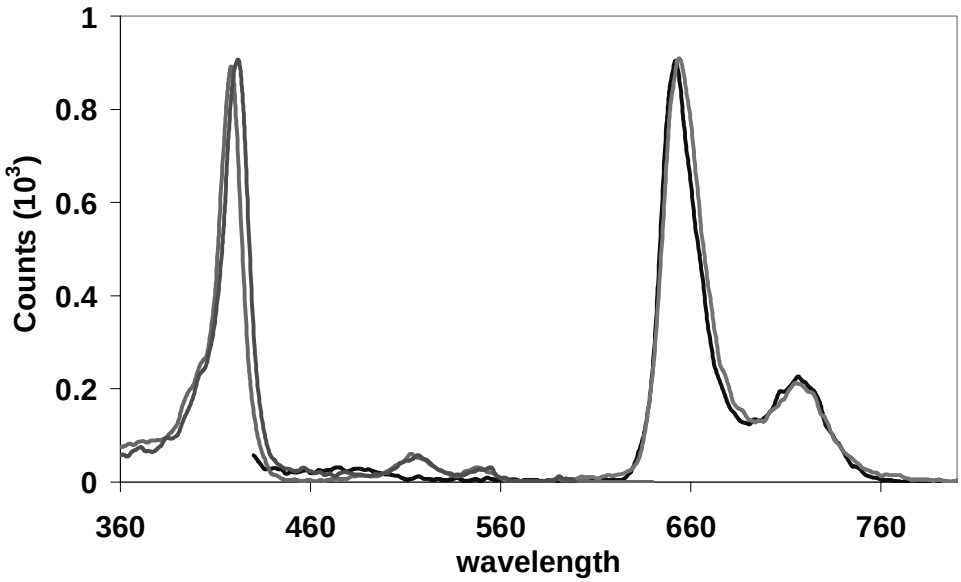

Figure 7: Fluorescence excitation (red line, TCPP; blue line, magnetite nanocrystal-TCPP) and emission (green line, TCPP; purple line, magnetite nanocrystal-TCPP) at pH 7. The excitation spectrum was detected at 651 nm, and the emission spectrum was excited at 418 nm.

When we carried out the same procedure with amorphous nanoparticles, the particles were first etched by the TCPP molecule before subsequent coating. This is revealed by TEM analysis, where the average particle size is reduced to 8 nm compared with 12 nm for untreated nanoparticles. Further evidence for this etching process is the formation of the green Fe(II)-porphyrin complex upon initial reaction with the amorphous nanoparticles. This is confirmed by ^{1}H NMR, where the presence of paramagnetic Fe(II) causes the shift and line broadening in the spectrum.

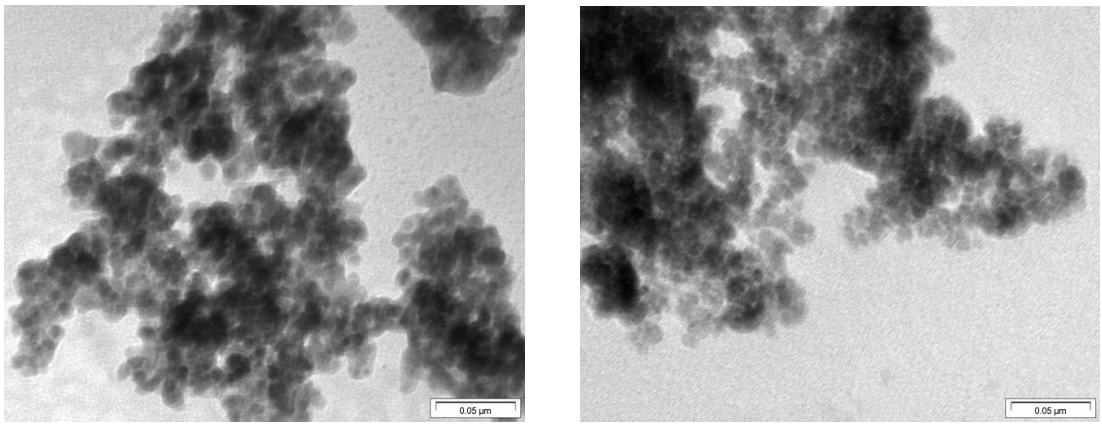

Figure 8: TEM images of amorphous nanoparticles (a) before and (b) after reaction with TCPP

3. EXPERIMENTAL

3.1. General procedures

All manipulations were carried out under vacuum or argon by Schlenk techniques. Organic solvents were dried and distilled over a sodium-potassium alloy under argon prior to use and then condensed into a reaction flask under vacuum shortly before use. Sodium tert-butoxide ($NaOBu^t$), iron (II) bromide ($FeBr_2$), 4, 4', 4'', 4'''-(21H, 23H-porphine-15, 10, 15, 20-tetrayl) tetrakis (benzoic acid) were all obtained from Aldrich. IR spectra (200-4000cm^{-1}) were recorded by

diffuse reflectance using a Perkin Elmer Spectrum One FT-IR spectrophotometer. The scanning electron microscopy (SEM) images of the samples were obtained using a Hitachi S-4300 scanning electron microscope, which was operated at 5.0 kV. The transmission electron microscopy (TEM) images were taken on a Hitachi H-7000. The TEM was operated at a beam voltage of 100 kV. Samples for TEM were prepared by deposition and drying of a drop of the powder dispersed in ethanol or distilled water onto a formvar coated 400 mesh copper grid. UV-Visible absorption spectra (200-700nm) were recorded using a Cary 300 scan UV-Vis spectrophotometer. Fluorescence spectra were performed on a LS-50B Perkin Elmer luminescence spectrometer, with a 150W Xenon lamp.

3.2. Preparation and porphyrin functionalisation of magnetite nanocrystals

$NaOBu^t$ (12.7g, 132.14mmol) was added to $FeBr_2$ (9.42g, 43.6mmol) in dry THF (approx. 100mL). The mixture was stirred for 24 hours at room temperature and afforded a filtrate of $[(THF)NaFe(OBu^t)_3]_2$ and a precipitate of sodium bromide. The mixture was filtered and the precipitate was carefully hydrolysed by distilled water (60mL). The reaction vessel was placed in ultrasound for two hours. The black precipitate was filtered and washed with distilled water and ethanol and was dried under vacuum. The magnetic material was characterised via TEM, SEM, IR and Mössbauer spectroscopy. 4, 4', 4'', 4''',-(21H, 23H-Porphine-5, 10, 15, 20–tetrayl)tetrakis–(benzoic acid) (0.005g, 0.0063mmol) was added to a suspension of the particles in dry THF and was placed in ultrasound for one hour. The mixture was filtered and the black precipitate was dried under vacuum for one day.

3.3. Preparation and porphyrin functionalisation of amorphous magnetite nanoparticles

$NaOBu^t$ (0.42g, 4.32mmol) was added to $FeBr_2$ (0.46g, 2.13mmol) in dry THF (approx. 100mL). The mixture was stirred for 24 hours at room temperature and afforded a filtrate of $[Fe(OBu^t)_2(THF)_2]_2$ and a precipitate of sodium bromide. The mixture was then filtered. The precipitate was carefully hydrolysed by distilled water (40mL) and was placed in ultrasound (30 kHz, 130 W) at room temperature for two hours. The black precipitate was washed with distilled water and ethanol and was dried under vacuum. 4, 4', 4'', 4''',-(21H, 23H-Porphine-5, 10, 15, 20–tetrayl)tetrakis(benzoic acid) (0.005g, 0.0063 mmol) was added to a suspension of the precipitate in dry THF. The reaction vessel was placed in ultrasound for one hour. A green filtrate and black precipitate were formed. The filtrate was concentrated to give a green powder, which was analysed by ^1H NMR. The black precipitate was dried under vacuum for one day.

4. CONCLUSIONS

Thus we have prepared new magnetic-fluorescent nanocomposites using TCPP and magnetite nanocrystals. We have found that the success of this process depends on the nature of the particles (crystalline or amorphous) used. The interaction of magnetite nanocrystals with TCPP gave stable core-shell composites which display fluorescent properties. However, in the case of amorphous particles the reaction with TCPP resulted in the etching of the nanoparticles and the formation of non-luminescent nanocomposites. New nanocrystalline magnetite-porphyrin composites may be potentially used in biomedical research as assays and magnetic and fluorescent biolabels.

REFERENCES

1. Q.A. Pankhurst, J. Connolly, S.K. Jones, J. Dobson, *J. Phys. D: Appl. Phys.*, **36**, R167, (2003).
2. I. Šafařík, M. Šafaříková, *Monatsh. Chem.*, **133**, 737, (2002).
3. C. Bergemann, D. Müller-Schulte, J. Oster, L. à Brassard, A.S. Lübbe, *J. Magn. Magn. Mater.*, **194**, 45, (1999).
4. R. N. Muller, A. Roch, J-M. Colet, A. Ouakssim, P. Gillis. *The Chemistry of Contrast Agents in Medical Magnetic Resonance Imaging*, A. E. Merbach, E. Toth, Eds.; John Wiley and Sons Publishers, p.417, (2001).
5. D.K. Kim, Y. Zhang, J. Kehr, T. Klason, B. Bjelke, M. Muhammed, *J. Magn. Magn. Mater.*, **225**, 256, (2001).
6. A. Jordan, R. Scholz, P. Wust, H. Fähling, R. Felix, *J. Magn. Magn. Mater.*, **201**, 413, (1999).
7. A. Jordan, R. Scholz, K. Maier-Hauff, M. Johannsen, P. Wust, J. Nadobny, H. Schirra, H. Schmidt, S. Deger, S. Loening, W. Lanksch, R. Felix, *J. Magn. Magn. Mater.*, **225**, 118, (2001).
8. E. Klarreich, *Nature*, **413**, 450, (2001).

9. H. Mattoussi, J.M. Mauro, E.R. Goldman, G.P. Anderson, V.C. Sundar, F.V. Mikulec, M.G. Bawendi, *J. Am. Chem. Soc.*, **122**, 12142, (2000).
10. B. Balou, B.C. Lagerholm, L.A. Ernst, M.P. Bruchez, A.S. Waggoner, *Bioconjugate Chem.*, **15**, 79, (2004).
11. M. Han, X. Gao, J.Z. Su, S. Nie, *Nat. Biotechnol.*, **19**, 631, (2001).
12. R. Bonnett, *Chem. Soc. Rev.*, **1**, 19, (1995).
13. I Cecic, M. Korbelik, *Cancer Lett.*, **183**, 43, (2002).
14. M. Šafaříková, I. Šafařík, *Eur. Cell. Mater.*, **3**, 188, (2002).
15. I. Šafařík, M. Šafaříková, *Sep. Sci. Technol.*, **32**, 2385, (1997).
16. Y.S. Kang, S. Risbud, J.F. Rabolt, P. Stroeve, *Chem. Mater.*, **8**, 2209, (1996).
17. X. Cao, Yu. Koltypin, G. Katabi, R. Prozorov, I. Felner, A. Gedanken, *J. Mater. Chem.*, **7**, 1007, (1997).
18. P. Tartaj, M. del Puerto Morales, A. Veintemillas-Verdaguer, T. González-Carreño, C.J. Serna, *J. Phys. D: Appl. Phys.*, **36**, R182, (2003).
19. Y.K. Gun'ko, U. Cristmann, V.G. Kessler, *Eur. J. Inorg. Chem*, **5**, 1029, (2002).
20. S.A. Corr, Y.K. Gun'ko, A.P. Douvalis, M. Venkatesan, R.D. Gunning, *J. Mater. Chem.*, **14**, 944, (2004).
21. G.B. Biddlecombe, Y.K. Gun'ko, J.M. Kelly, S.C. Pillai, J.M.D. Coey, M. Venkatesan, A.P. Douvalis, *J. Mat. Chem.*, **11**, 2937, (2001).